Journal of Physics D: Applied Physics

PAPER

Effects of non-equilibrium excitation on methane oxidation in a low-temperature RF discharge

To cite this article: Jintao Sun *et al* 2020 *J. Phys. D: Appl. Phys.* **53** 064001

IOP Publishing Journal of Physics D: Applied Physics

J. Phys. D: Appl. Phys. **53** (2020) 064001 (13pp) https://doi.org/10.1088/1361-6463/ab57dc

Effects of non-equilibrium excitation on methane oxidation in a low-temperature RF discharge

Jintao Sun[1], Qi Chen[1], Xiaofang Yang[2] and Bruce E Koel[2]

[1] School of Mechanical, Electronic and Control Engineering, Beijing Jiaotong University, Beijing 100044, People's Republic of China
[2] Department of Chemical and Biological Engineering, Princeton University, NJ 08544, United States of America

E-mail: qchen@bjtu.edu.cn (Q Chen)

Received 30 July 2019, revised 7 November 2019
Accepted for publication 14 November 2019
Published 4 December 2019

Abstract

The kinetic effects of non-equilibrium excitation by direct electron impact on low-temperature oxidation of CH_4 were investigated by experiment and simulation. We focused on the vibrational-electronic-chemistry coupling of methane and oxygen molecules under conditions of immediate reduced electric field strengths of 30–100 Td in an RF dielectric barrier discharge. A detailed plasma chemistry mechanism governing the oxidation processes in an $He/CH_4/O_2$ combustible mixture was proposed and studied by including a set of electron impact reactions, dissociative recombination reactions, reactions involving vibrationally- and electronically- excited species, and important three-body recombination reactions. A linear increase in reactant consumption with an increase in plasma power was observed experimentally. This suggested the presence of decoupling between the molecular excitation by plasma and the low-temperature chemistry. However, CO formation showed a non-linear trend, with its formation increasing with lower energy inputs and decreasing at higher energy inputs. By modelling the chemical kinetic sensitivity and reaction pathways, we found that the formation of radicals via the chain propagation reactions $CH_4 + O(^1D) \rightarrow CH_3 + OH$, and $O_2(a^1\Delta_g) + H \rightarrow O + OH$ was mainly accelerated by the electronically excited species $O(^1D)$ and $O_2(a^1\Delta_g)$. The numerical simulation also revealed that under conditions of incomplete relaxation, the vibrational species $CH_4(v)$ and $O_2(v)$ enhanced chain propagating reactions, such as $CH_4(v) + O \rightarrow CH_3 + OH$, $CH_4(v) + OH \rightarrow CH_3 + H_2O$, $O_2(v) + H \rightarrow O + OH$, thus stimulating the production of active radicals and final products. Specifically, for an *E/N* value of 68.2 Td in a stoichiometric mixture (0.05 CH_4/0.1 O_2/0.85 He), $O(^1D)$, $CH_4(v13)$, and $O_2(v)$ were estimated to contribute to 12.7%, 3.6%, and 3.8% of the production of OH radicals respectively. The reaction channel $CH_4(v13) + OH \rightarrow H_2O + CH_3$ was estimated to be responsible for 1.6% of the H_2O formation. These results highlight the strong roles of vibrational states in a complex plasma chemistry system and provide new insights into the roles of excited species in the low-temperature oxidation kinetics of methane.

Keywords: RF discharge, vibrational excitation, non-equilibrium excitation, plasma-assisted combustion, low-temperature chemistry, sensitivity analysis

S Supplementary material for this article is available online

(Some figures may appear in colour only in the online journal)

1. Introduction

Plasma-assisted ignition and combustion, which are widely applied in gas turbines, scramjets, and internal combustion engines [1–3], has been considered as a promising technique in shortening ignition delay time, improving combustion energy efficiency, and reducing emission. As non-equilibrium plasmas can excite gas molecules to higher energy states or directly dissociate the molecules, they have the potential to produce reactive species at residence time and location in a combustible mixture; furthermore, they efficiently accelerate the overall pyrolysis, oxidation, and ignition. Previous studies have demonstrated the effectiveness of plasma-assisted combustion by using DC [4], AC [5], microwave [6], radio frequency [7, 8], and nanosecond pulsed discharge [9–11]. Owing to the complicated interaction between plasma and combustion in different types of plasmas, detailed plasma-combustion chemistry is still not well understood. It remains unclear how the reduced electric fields control the low-temperature non-equilibrium excitation and how the excited species, especially the vibrationally excited species enhance the low-temperature chemistry in a well-defined discharge environment.

A prominent aspect of the electric discharge impact in a combustible mixture is that various degrees of freedom of molecules are excited [1–3]. The types of plasma-excited species are strongly dependent on the reduced electric field strength *E*/*N*. At high *E*/*N*, such as in an NSD discharge, dissociation and ionization of molecules dominate the discharge processes. At intermediate or low *E*/*N*, such as in an RF discharge, vibrationally- and electronically- excited species are largely produced [12]. Obviously, non-equilibrium molecular excitation can effectively compete with the dissociation and ionization of molecules, and thus becomes the important process in a discharge mixture with intermediate or low reduced electric field values. The present work focuses on the effects of non-equilibrium excitation by direct electron impact on low-temperature oxidation of CH_4 under conditions of immediate *E*/*N* of 30–100 Td in an RF dielectric discharge.

Excited species generated in high *E*/*N* plasma and their effects on ignition and combustion have been studied extensively by advanced diagnostics in the past years. Singlet delta oxygen $O_2(a^1\Delta_g)$ is an electronically excited O_2 to its first electronically excited low-energy level at 0.98 eV, and it has a higher oxidation potential than the ground state O_2. Ombrello *et al* measured the absolute concentrations of $O_2(a^1\Delta_g)$ by the integrated cavity output spectroscopy (ICOS) [13]. They found that $O_2(a^1\Delta_g)$ participated in both chain initiation and chain branching reactions [14]. Uddi *et al* measured atomic O in a nanosecond discharge using the two photon laser induced fluorescence (TALIF) [15]. Their work suggested that atomic O was primarily formed both from electron impact reactions during the discharge and from the collisions of electronically excited N_2 with O_2. $O(^1D)$ is electronically excited by plasma and has a long lifetime, thus it has the high reactivity needed to react with all hydrocarbons and molecular hydrogen, even at room temperature conditions. Starikovskaia *et al* used the unfocused laser radiation to uniformly excite the combustible mixture by volume nanosecond discharge and found that additions of $O(^1D)$ significantly reduced the induction times [16]. The influence of $O(^1D)$ on fuel oxidation has been further studied by Popov [17]. He found that $O(^1D)$ reacted with fuel molecules by rapid production of radicals at the relatively low temperatures. Concerning vibrationally-excited species, Stancu *et al* quantified electronically excited N_2 (N_2(A3), N_2 (B3), and N_2(C3)) in a pin-to-pin nanosecond pulsed discharge using cavity ring-down spectroscopy (CRDS) [18]. Adamovich and co-workers measured vibrationally excited nitrogen $N_2(v)$ using coherent anti-stokes Raman spectroscopy (CARS) [19, 20]. Their results revealed that, in 10 kHz repetitively pulsed plane-to-plane plasmas, up to 50% of the coupled discharge power causes molecular vibrational excitation, which is in good agreement with a master equation kinetic model.

Accordingly, the plasma-chemistry system is complicated by the different types of excited species and the reactions involving these excited species. Kinetic analysis is often performed together with theoretical studies and numerical modelling. For example, Starik *et al* developed theoretical approaches and chemical kinetic models for combustion reactions involving methane, syngas, ethane, and hydrogen by considering excited species [21–24]. The results revealed that the pre-excitation of the vibrations of H_2, N_2, and CO molecules significantly enhanced the ignition of a syngas-air mixture in a supersonic flow owing to the increase in the elementary reaction rate of gas molecule decomposition. Tsolas *et al* numerically investigated the kinetics of plasma-assisted pyrolysis and oxidation of C_2H_4, showing that direct collisional quenching of electronically excited argon by ethylene is responsible for the low temperature enhancement of fuel consumption seen in an NSD plasma-assisted pyrolysis experiment [25]. DeFilippo *et al* developed a detailed chemical kinetic reaction mechanism for CH_4 combustion with relevant plasma reactions that could be applied to both high- and low-energy excitation [26]. Sensitivity analysis of model predictions to elementary reaction rate highlighted the increased importance of charge balance reactions as well as energy loss to nitrogen vibrational excitation. Nevertheless, the effect of vibrational excitation on ignition was not mentioned in the published results. In addition, recently, the effects of controlled non-equilibrium excitation of reactant molecules on low temperature ignition in CH_4/O_2/He and H_2/O_2/He mixtures using a hybrid repetitive nanosecond (NSD) and DC discharge at atmospheric pressure was studied numerically. Selective non-equilibrium excitation of vibrationally excited $H_2(v)$ and $O_2(v)$ as well as electronically excited $O_2(a^1\Delta_g)$ and $O(^1D)$ have been considered and the kinetic roles of these active species have been addressed [27, 28]. Different kinetic mechanisms were developed to model the plasma-assisted ignition enhancement and plasma-assisted fuel oxidation. Most of the studies have focused on the non-equilibrium excitation in a high *E*/*N* discharge. Despite the earnest efforts above, the kinetic mechanism of molecular excitation, especially the vibrational excitation during the fuel oxidation and ignition by low *E*/*N* discharge is not well understood. Therefore, to understand the detailed kinetic enhancement at relatively lower *E*/*N* and low temperatures, mechanisms involving molecular excitation, especially

vibrational excitation, and its kinetic effect on fuel oxidation and ignition in a well-defined low *E/N* discharge system are greatly needed [19, 29, 30].

In this report, we used experiments and computations to study the kinetic processes involving vibrational and electronic excitations of gas molecules in a relatively lower *E/N* RF plasma-assisted CH_4 oxidation system with varying temperatures. The conversion of O_2 and CH_4, and the product yields were analyzed from the results in a flow plasma reactor with the gas compositions measured by on-line gas chromatography (GC-TCD). The experimental data were then used to validate the kinetic model. Kinetic insights of the overall active species, including vibrational and electronic states on the plasma-assisted methane pyrolysis and oxidation were obtained based on the discussion of reaction pathways, as well as a temporal sensitivity analysis. Together with species profiles, in-depth insight into the major kinetics was proposed, including rate-limiting steps, competing steps, and excitation and relaxation of the excited species.

2. Experimental methods and kinetic modelling

2.1. Methane pyrolysis and oxidation system with RF discharge

The experimental setup used in this study, which was previously described in other works [31], is shown in figure 1(a). The experimental setup mainly consists of a wire-cylinder dielectric barrier discharge (DBD) reactor, an RF power supply, gas mass flow controls, high voltage probes, and a GC-TCD measurement system. The DBD flow reactor was a cylindrical glass vessel with 10 mm I.D. and 12 mm O.D. The copper high-voltage electrode was pre-loaded into a quartz tube with 3 mm I.D. and 4 mm O.D., and was then positioned in the center of the DBD flow reactor. The ground electrode was a 19 mm length copper tube, tightly attached to the outer wall of the quartz tube. All experiments were conducted under a total pressure of 100 Torr. The reaction temperatures were controlled at 473 or 673 K. A tube furnace (Lindberg/Blue) was used to heat the reactor from outside for achieving the desired reaction temperature of the reaction gases. A Type-K thermocouple probe ($\pm$1 K) with a diameter of 1 mm was located at the end of the reaction zone after plasma discharge to measure the mixture temperature. The highly diluted CH_4–O_2 mixture in helium was chosen to lower breakdown voltages and to reduce the streamers formation. The gas flow rate was set at 100 sccm with the flow controlled by mass flow controllers. Two gas mixtures were used: 0.05 CH_4, 0.1 O_2, 0.85 He, and 0.05 CH_4, 0.2 O_2, 0.75 He. The helium premixed combustible mixtures was adjusted to have equivalent ratios φ of 1 and 0.5 in CH_4/O_2. The electrode edges were polished to avoid the local enhancement of electric field and dielectric breakdown [32]. The high-voltage electrode shown in figure 1(a) is connected to a Ceaser RF Power Generator, which could supply a maximum sine-wave voltage and current of 4 kV and 1.5 A, respectively, and a frequency of 13.56 MHz with an automatic impedance matching network. The RF power in the range of 20–90 W was used in this study. Good plasma stability and impedance matching can be achieved with less than 1% of the input RF power reflected back.

The applied voltage and discharge current were measured by a digital oscilloscope (Tektronix DPO 7410C) together with a Lecroy high voltage probe (PPE20KV) and a Pearson Coil current probe (Model 6585), respectively. A simplified model of the reactor equivalent electrical circuit in figure 1(b) is used to calculate the reduced electric field *E/N* as a function of the applied voltage, the discharge gap, and the reaction temperature downstream of the discharge. An *E/N* of 30–100 Td in the continuous RF discharges under experimental conditions was determined. The peak–peak voltage and the variation in *E/N* with RF power was plotted for $He/CH_4/O_2$ plasmas (figure 2). The measured voltages as well as the calculated *E/N* values show a nonlinear trend with RF power-input, suggesting the existence of coupling between the discharge behavior and the matched electrical circuit. The reactants and major products, i.e. CH_4, O_2, CO, CO_2, CH_2O, CH_3OH, H_2O, H_2, C_2, and C_3 hydrocarbons species from the plasma-assisted methane conversion were quantified by using a micro GC system (INFICON 3000). The calibrations were performed by conveying a sample gas with known species concentrations through the GC at conditions identical to those of the experiments. The relative mole fraction uncertainties of the species in the gas sample were found to be less than $\pm$5%.

2.2. Computational approach with a plasma-assisted combustion kinetic model

A 0D plasma-chemistry globe model was used to explore the detailed plasma chemistry in an $He/CH_4/O_2$ mixture discharge [31]. The model integrates the electron Boltzmann equation solver Bolsig+ and the chemical kinetics solver CHEMKIN. The rate coefficients of the electron impact elementary reactions were calculated on Bolsig+ by solving the steady state, two-term expansion Boltzmann equation. The cross sections of electron elastic impact and, electron excitation and dissociation used in this study were obtained from the online LXCAT (Plasma Data Exchange Project) database [33] and the literature [34, 35]. Then, they were integrated over the electron energy distribution function (EEDF) to obtain the rate coefficients of the electron involving reactions. Time evolution of species production and consumption in a low pressure well-mixed reactor with non-equilibrium plasma processing was solved on the Plasma-PSR module in CHEMKIN.

Temporal evolution of the electrons, free radicals, charged species, excited species, including electronically and vibrationally excited species, and the final products was calculated by a set of conversion equations such as the charge balance equation, species conservation equation, energy conservation equation, and state equation. The species included in this kinetic model are shown in table 1. Transport processes were not taken into account during the modelling. The Poisson equation for the electric field was not solved during the kinetic modelling, and the charge separation and sheath formation near the electrodes was therefore neglected. The retention time in which the gas molecules travel through the reactor was set the same as the experimental measurement [21]. The reduced

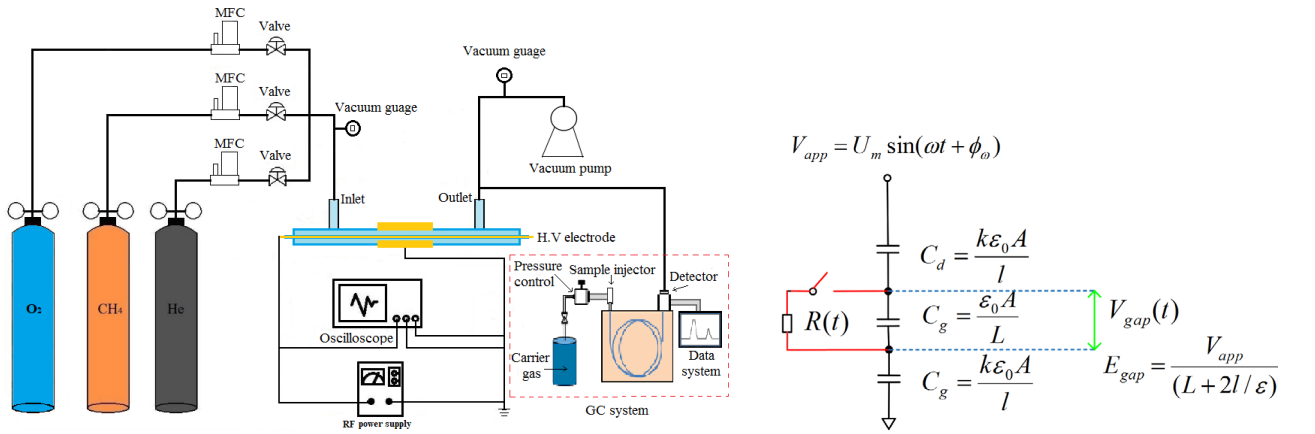

Figure 1. Schematic diagram of (a) experimental setup and (b) layout of the DBD reactor equivalent circuit. C_d is the capacitance of the dielectric layers, C_g is the capacitance of the air gap, V_{app} is the voltage applied to the electrodes, and R is the equivalent resistance of the DBD discharge. Here, A is the electrode area, l is the thickness of the dielectric layer, k is the dielectric constant, and L is the discharge gap width. The reduced electric field is calculated as a function of the applied voltage, V_{app}, and the discharge gap, L.

electric field E/N was considered as an adjustable parameter to fit the methane conversion rate in the experimental results owing to the strong sensitivity of the reaction rates of methane dissociation ionization to the electron density and electron energy distribution. The resulting reduced electric field was within 10% discrepancy from the reduced electric field values determined by the measured average applied voltage, the discharge channel distance, the quartz layer thickness, and the dielectric constant, as shown in figure 2.

A set of elementary reactions was modelled for methane pyrolysis and oxidation in RF discharge plasma. The comprehensive combustion model, HP-Mech, which was developed at Princeton [36, 37], modelled the rate coefficients of radical/ion reactions, which govern the kinetic process of plasma-assisted low and high temperature chemistry. Other reactions were integrated to describe the evolution of a plasma combustion system, including electron impact reactions involving vibrationally- and electronically-excited species, ion–ion exchange reactions, electron–ion recombination reactions, and reactions involving excited particles. The reaction set used in this study is an extension of our recently published work [31]. The main improvement of the model is the addition of a complex set of vibrationally excited species, i.e. CH_4(v13), CH_4(v24), O_2(v1), O_2(v2), O_2(v3), and O_2(v4). In vibrational energy relaxation reactions, the vibrational energy is either lost to translational degrees of freedom (VT relaxation), or exchanged among two vibrational modes (VV′ relaxation) or two molecules in the same mode of vibration (VV relaxation). The rate coefficients of VV and VT relaxations are obtained from [2, 38, 39]. The rate coefficient for key elementary chemical reactions involving vibrational species can be calculated by the theoretical-information approach [40].

$$k_R\left(E_v, T_0\right) = k_{R0} \exp\left(-\frac{E_a - \alpha E_v}{T_0}\right) \theta\left(E_a - \alpha E_v\right). \quad (1)$$

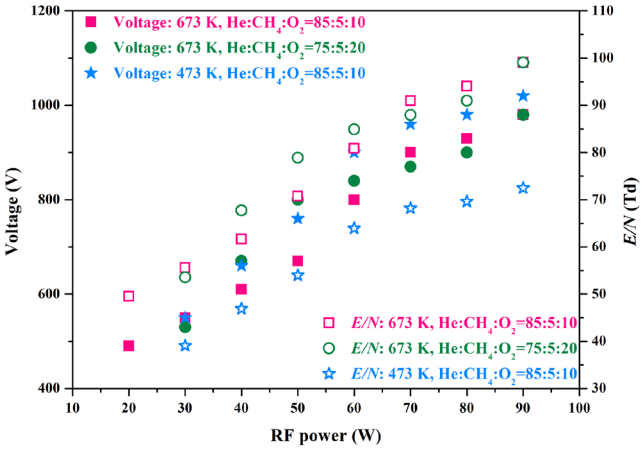

Figure 2. Peak voltage on electrodes and E/N ratios under different RF powers for He/CH_4/O_2 plasmas. The calculated reduced electric field value is based on the measured average voltage applied on the electrodes, the discharge gap distance, the quartz layer thickness, the dielectric constant, and the temperature measured by a thermocouple placed downstream of the discharge.

Here, k_{R0} is the pre-exponential factor, T_0 is the translational gas temperature, E_a is the activation barrier for the chemical reaction, E_v is the vibrational energy of a vibrationally-excited molecule, and $\theta(x)$ is the Heaviside step function ($\theta(x) = 1$ when $x \geqslant 0$; and $\theta(x) = 0$ when $x < 0$).

The coefficient α for the efficiency of vibrational energy can be calculated based on the Fridman–Macheret α-Model [12]:

$$\alpha = \frac{E_a^{(f)}}{E_a^{(f)} + E_a^{(b)}}. \quad (2)$$

The subscript f and b stand for forward and backward reactions. As a result, the numerical model included 95 species, and 1781 elementary reactions.

Table 1. Free radicals, charged and excited species, and final products included in numerical modelling.

Species type	Symbol	Number
Reactants	He, CH_4, O_2	3
Molecules	H_2, O_2, H_2O, He, H_2O_2, O_3, CO, CO_2, CH_2O, CH_3OH, CH_3O_2H, CH_4, C, C_2H_6, C_2H_4, C_2H_2, CH_3CHO, C_2H_5OH, OCHCHO, aC_3H_4, pC_3H_4, c-C_3H_4, C_3H_6, C_3H_8, C_2H_3CHO, CH_2CO, HCCOH, $C_2H_4O_1$-2, HOCHO	29
Radicals	H, O, OH, HO_2, HCO, CH_2OH, CH_3O, CH_3O_2, CH_3, CH_2, CH_2(S), CH, C_2H_5, C_2H_3, C_2H, CH_2CHO, HCCO, H_2CC, C_2O, C_2H_5O, CH_2CH_2OH, CH_3CHOH, $C_2H_5O_2$, $C_2H_3O_1$-2, CH_2CHOH, $C_2H_3O_2$, CH_3OCH_2, C_3H_3, aC_3H_5, tC3H5, sC_3H_5, nC_3H_7, iC_3H_7, C_2H_3CO, CH_3CO, HOCO, OCHO, HCOH	38
Excited species	He(2^3S), O(^{1}S), O(^{1}D), $O_2(a^1\Delta_g)$, $O_2(b^1\Sigma_g^+)$, O_2(A3), O_2(v1), O_2(v2), O_2(v3), O_2(v4), CH_4(v24), CH_4(v13)	12
Charged species	e, He^+, CH_5^+, CH_4^+, CH_3^+, CH_2^+, H_2^+, H^+, O_2^+, O^+, O_2^-, O^-, H_2O^+, OH^+, OH^-, H^-	16

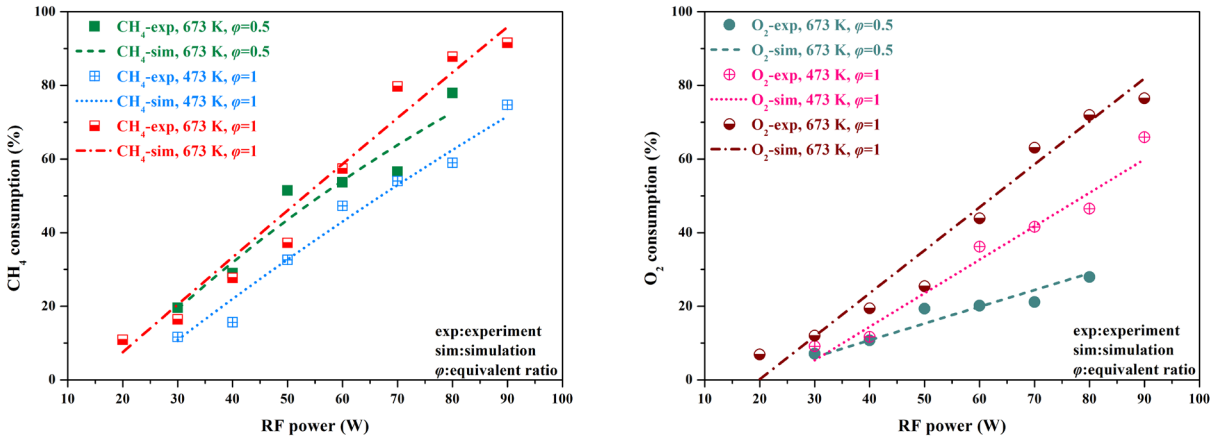

(a) (b)

Figure 3. Steady state measurements and modelling of CH_4 and O_2 consumption for 0.85:0.05:0.1 ($\varphi = 1$) and 0.75:0.05:0.2 ($\varphi = 0.5$) He/CH_4/O_2 mixtures at temperatures of 473 and 673 K, respectively.

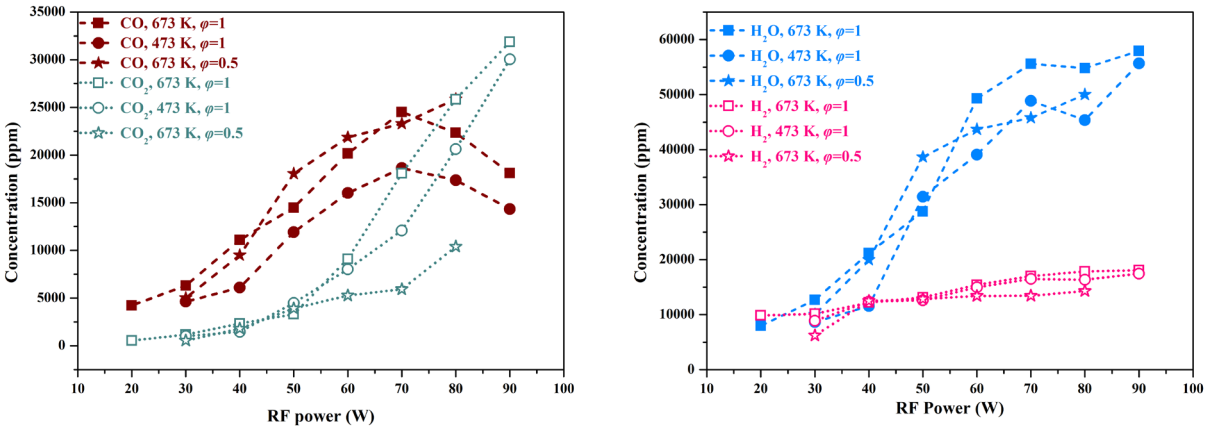

(a) (b)

Figure 4. Steady state measurements of major species for (a) CO and CO_2 and (b) H_2O and H_2 for 0.85:0.05:0.1 ($\varphi = 1$) and 0.75:0.05:0.2 ($\varphi = 0.5$) He/CH_4/O_2 mixtures at downstream temperatures of 473 and 673 K, respectively.

3. Results and discussion

3.1. RF plasma-assisted methane pyrolysis and oxidation

Steady state measurements for methane and oxygen consumption, and key species generation were performed to explore low temperature plasma-initiated reaction pathways at intermediate *E*/*N* values of 30–100 Td. Under this electrical field, both vibrational and electronic excitation, and dissociative excitation are important for the reactions. Different dilution levels in the gas mixtures were chosen to study the sensitivity of the reaction to excess O_2. As shown in figure 3, methane and O_2 conversions linearly increase with the plasma power, highlighting the strong correlation between the molecular excitations and energy input. The equivalent ratio φ and the reaction temperatures also greatly affect CH_4 and O_2

consumption. The decrease in the equivalent ratio φ from 1 to 0.5 doubles the O_2 concentrations in the gas mixture, which alters the energy branching for various elementary reactions, influencing CH_4 and O_2 consumption. This is mainly because the energy disposition depends on not only the reduced electric field but also the gas composition [12].

The CH_4 and O_2 consumption by RF plasma was simulated with the results shown by dashed lines in figure 3. The CH_4 consumption and O_2 consumption in the range of 20–90 W RF power are consistent with the experimental results, with an error less than 5%. This value is within the experimental uncertainty. As the reactants consumption is almost entirely caused by electron collision reactions and quenching of excited species [11], the agreement between the modelling and experimental results for CH_4 and O_2 consumptions in this study strongly indicates that the related electron collision reaction rates, including vibrational, electronic excitation, dissociation, and ionization, have been well modelled.

The steady state production of major species, including CO and CO_2, H_2O, and H_2 is shown in figure 4. Water is produced in the greatest quantity, followed by carbon monoxide, hydrocarbon, and carbon dioxide. A non-linear trend in CO formation, i.e. increasing at lower input energy but decreasing at higher energy input, suggests that branching factors contribute to its formation. The large increase in the production of CO_2 at a high plasma energy input (70–90 W) can be explained by the higher power plasma-promoted CO conversion into CO_2. The dominant pathway reported for CO_2 formation is the CO oxidation reaction: $CO + OH \rightarrow CO_2 + H$ [41]. A sharp increase in OH radicals with increasing *E/N* is thereby expected to accelerate the oxidation rate. H_2 and H_2O formation is another major pathway for methane pyrolysis and oxidation by plasma. Linear increases in H_2O and H_2 formation with increasing plasma energy input was observed. This is most likely due to the H-abstraction reaction of methane, which produces more OH and H radicals at higher *E/N* values.

The effect of helium under $\varphi = 1$ and $\varphi = 0.5$ on the formation of major species is compared in figures 4(a) and (b). An increase in CO_2, H_2O, and H_2 production is consistent with the larger consumption of CH_4 and O_2 shown in figure 3. The thermal effect for the downstream temperatures of 473 and 673 K was also compared in figure 4. The higher gas temperature was found to promote the production of major species in plasma-assisted pyrolysis and oxidation. An overall carbon balance of 90% or greater was maintained for all experiments in this study. The unbalanced carbons should exist as higher hydrocarbons or carbon deposits.

The concentrations of minor products, i.e. CH_2O and C_2H_6, are plotted in figure 5. C_2H_4, C_3H_6, and C_3H_8 species with less than 100 ppm mole fractions were observed but not included in this figure. Several other minor species were also formed in the plasma, namely, C_2H_2, C_3H_4, and acetaldehyde (CH_3CHO). As shown in figure 5, higher plasma energy input largely inhibits CH_2O formation. The dominant consumption pathway reported for CH_2O in plasma-assisted methane oxidation is $CH_2O + OH \rightarrow H_2O + HCO$ [11]. Therefore, a decrease in CH_2O formation with increasing plasma energy is

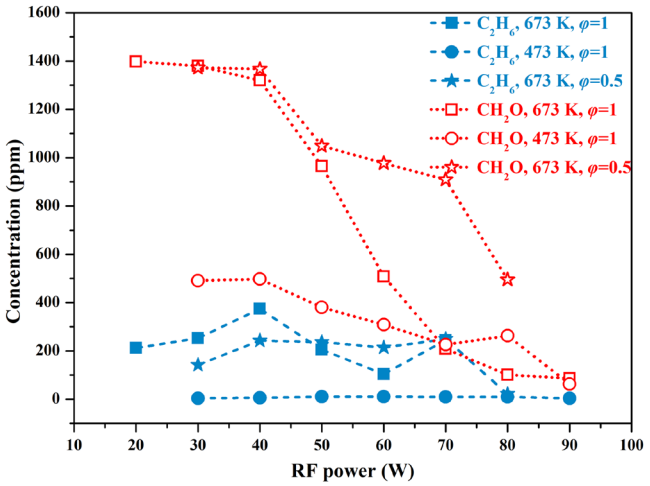

Figure 5. Steady state measurements of minor species for CH_2O and C_2H_6 species in 0.85:0.05:0.1 ($\varphi = 1$) and 0.75:0.05:0.2 ($\varphi = 0.5$) He/CH_4/O_2 mixtures at downstream temperatures of 473 and 673 K, respectively.

consistent with the H_2O formation trend in figure 4(b). On the other hand, the main reaction pathway for CH_2O formation is the oxidation of fuel or fuel fragments by plasma generated O and $O(^1D)$ atoms. As such, large concentrations of O and $O(^1D)$ atoms in a low equivalent-ratio He/CH_4/O_2 mixture lead to a dramatic increase in the CH_2O formation.

Figure 6 compares the model predicted and the GC measured concentrations for major products, i.e. CO, CO_2, H_2O, and H_2, as well as minor products, i.e. C_2H_6, CH_2O, and CH_3OH. The kinetic model predicted H_2O, CO, and CH_2O formation with good accuracy for all experimental cases, where the maximum deviation between the predicted and measured values was within 7.6%, 27.3%, and 12.7% for H_2O, CO and CH_2O, respectively. This model captures the correct trend of H_2, but considerably under-predicts the absolute concentration (a maximum deviation of 60%), probably owing to the over-estimation of the measured concentration, which is caused by the strong overlapping peaks for H_2 and He in GC measurements. Note that hydrogen is produced in large quantities at relatively low power and does not significantly change as the power is increased over the entire range. This is the result of the large consumption of hydrogen by the growing oxygen atom production with increasing power. Moreover, the CH_3OH concentration is over-predicted, and the maximum error is 61.2%, indicating that this is the major limitation in the model's predictive ability of this primary intermediate. The formation pathway reported for CH_3OH in an He/CH_4/O_2 combustible mixture is $CH_3O_2 + OH \rightarrow CH_3OH + O_2$. On the other hand, CH_3O_2 primarily comes from CH_3, $CH_3 + O_2(+M) \rightarrow CH_3O_2(+M)$. Thus, to improve the model prediction of methanol, the consumption and/or formation reactions of CH_3 need to be improved. In summary, the major trends of reactant consumption and major product formation are predicted well by the model, indicating that the modelled electron collision rates and dominant reaction pathways are quite accurate.

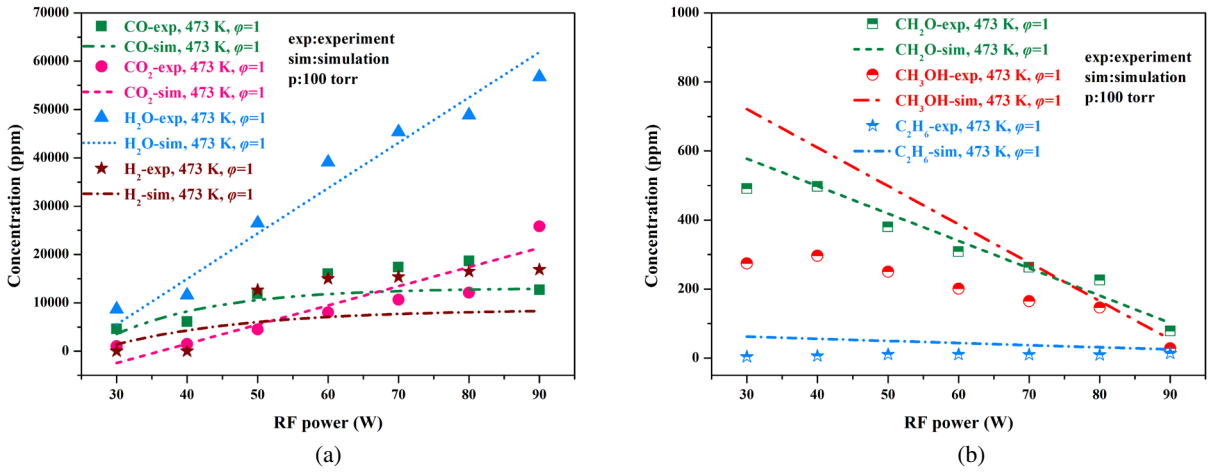

Figure 6. Comparisons of species concentration between experimental and modelling results in an $He/CH_4/O_2$ combustible mixture as a function of RF power: (a) CO, CO_2, H_2O, and H_2, and (b) CH_2O, CH_3OH, and C_2H_6.

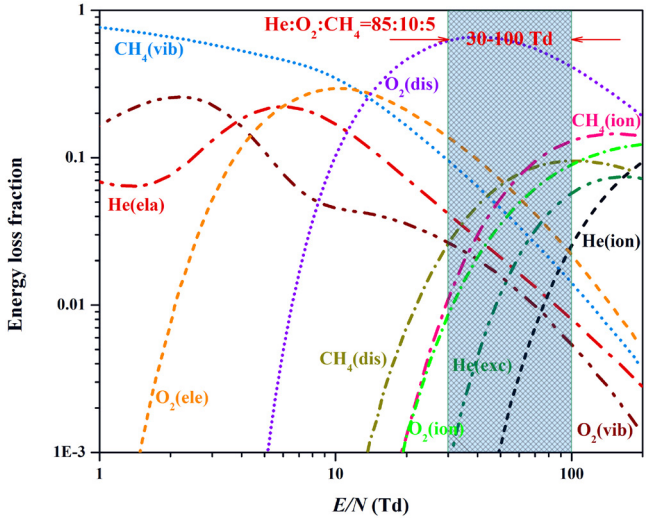

Figure 7. Fractional power dissipated by electrons into the different molecular degrees of freedom. Gas composition: 0.85 He/0.05 CH_4/0.1 O_2.

3.2. Impact of molecular excitation on methane oxidation

E/N is an important parameter controlling the direction of energy deposition and molecular excitation, dissociation, and ionization in a plasma. Energy branches at various reduced electric field *E/N* in a stoichiometric $He/CH_4/O_2$ discharge mixture are presented in figure 7. For a relatively lower reduced electric field (<10 Td), the most efficient mechanisms for electron energy loss are the elastic collisions of Helium and the vibrational excitations of methane and oxygen molecules. The vibrational excitation is very important at low *E/N* values. Between 10 and 100 Td, the dissociative excitation of oxygen molecule occurs at the highest energy loss fraction because of the low concentration of O_2 molecules and high average electron temperature in a highly diluted mixture; however, there is a considerable percentage of plasma energy transferred to the vibrational and electronic excitation of CH_4 and O_2. Thus, the vibrational and electronic excitation processes can effectively compete with the dissociation and ionization processes of gas molecules in this *E/N* value range. Furthermore, as the excited species can greatly lower the activation energy barrier, chemical reactions involving vibrational and electronic states usually affect the initial formation of active radicals, as well as molecules with single or few quanta [12].

Different elementary reactions occurring simultaneously in an RF discharge system contribute to the overall methane oxidation process. The reaction rate and reaction rate coefficient are the major collision parameters used to describe the kinetic processes. Specifically, for the elementary plasma-chemical reactions by electron impact, the reaction rate can be expressed as the integration of the reaction cross section or probability over the relevant distribution function, and is related to the reaction rate constant and concentration of the reactants. Correspondingly, the reaction rate constant is an integral factor that includes information about the reaction cross section and energy distribution functions, and strongly depends on the electron temperature or reduced electric field (*E/N*) [12]. Figure 8(a) shows the variation in the rate constants for key elementary reactions of CH_4 and O_2 gas molecules by electron impact in an $He/CH_4/O_2$ discharge system as a function of the reduced electric field. Below 10 Td, the rate constant for the vibrational excitation reaction of the CH_4 molecule, $e + CH_4 \rightarrow e + CH_4(v)$, can reach 10^{-8} cm^3 s^{-1}. This explains why a large fraction of electron energy in an RF discharge is available for vibrational excitation at low *E/N* values. With increasing *E/N*, electronic excitation of O_2 molecule becomes significant because of the high-energy threshold of this process, which leads to an abrupt increase in the rate coefficient of the elementary reaction by electronic excitation. The dissociative excitation of the elementary reaction $e + O_2 \rightarrow e + O + O(^1D)$ presents the most promising channel. This demonstrates the efficiency of oxygen atom production in an $He/CH_4/O_2$ discharge.

As described by the mass action law [41], the vibrational, electronic, and dissociative excitation of methane and oxygen in a plasma discharge are determined by the reaction rates of different elementary reactions, not by the rate constant. The reaction rates of different electron impact reactions are compared in figure 8(b). The results reveal that the dissociation of oxygen by electron impact, $e + O_2 \rightarrow e + O + O(^1D)$, is

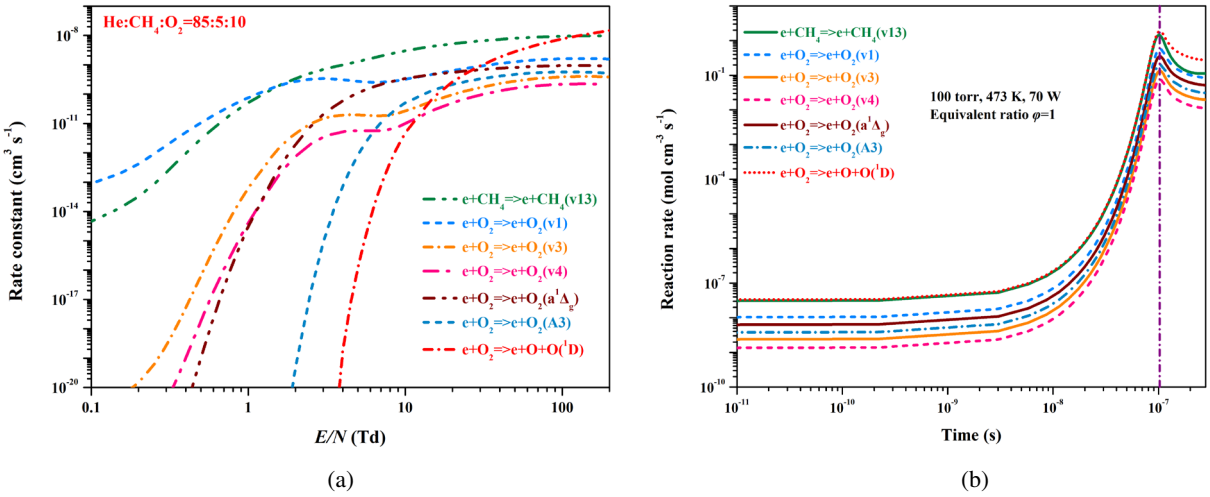

Figure 8. Reaction rate constants and reaction rates for elementary plasma-chemical reactions due to electron impact: (a) rate constant with an increasing *E*/*N* and, (b) reaction rate with time evolution in a stoichiometric mixture (0.05 CH_4/0.1 O_2/0.85 He) under a total pressure of 100 Torr and a temperature of 473 K with an *E*/*N* value of 68.2 Td.

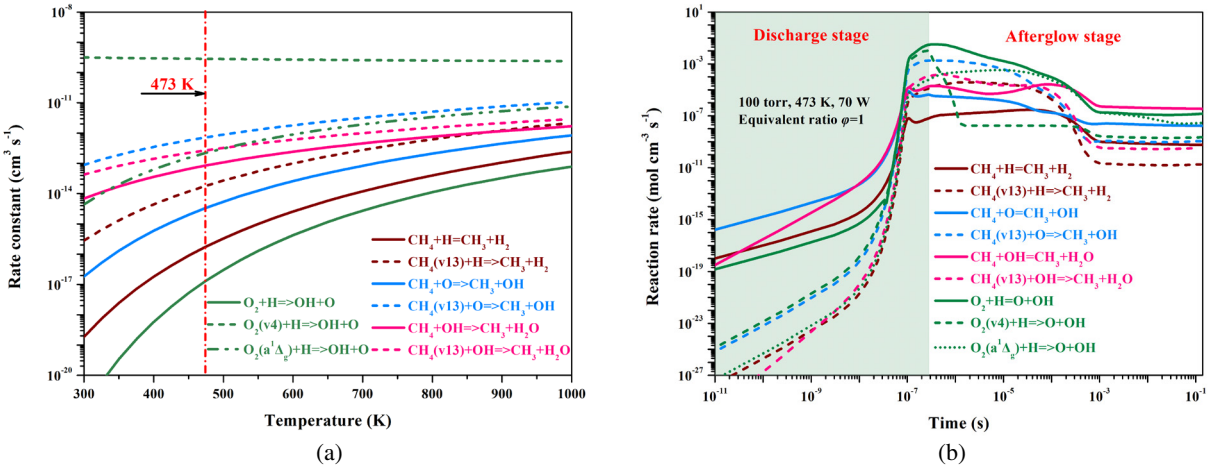

Figure 9. Reaction rate constants and reaction rates for typical chain branching reactions stimulated by excited molecules: (a) rate constant with increasing temperature and (b) reaction rate with time evolution in a stoichiometric mixture (0.05 CH_4/0.1 O_2/0.85 He) under a total pressure of 100 Torr and temperature of 473 K with an *E*/*N* value of 68.2 Td.

the fastest, followed by the vibrational excitation of methane, electronic excitation of oxygen, and finally vibrational excitation of oxygen. The difference in reaction rates for molecular excitation generates different excited species in the discharge afterglow.

Vibrationally and electronically excited species are able to make a significant contribution to plasma-chemical kinetics either owing to their high energy or their ability to suppress activation barriers of chemical reactions. The rate coefficient is a key parameter describing the influence of the plasma excitation of molecules on their chemical reaction rates [12]. As described in section 2.2, Fridman–Macheret α-Model was used to calculate the rate coefficient for key elementary chemical reactions involving vibrational species. As an example, in figure 9(a), the rate constant for the chain branching reaction stimulated by the vibrationally excited oxygen molecule $O_2(v4)$, $O_2(v4) + H \rightarrow OH + O$, is about 10^5–10^7 times faster than that of the conventional reaction $O_2 + H = OH + O$ in the temperature range of 473–673 K. As shown in figure 9(a), other excited species generated in a discharge, such as the electronically excited species $O_2(a^1\Delta_g)$ and vibrationally excited species $CH_4(v13)$, participate in molecule-radical reactions, and increase the reaction rate constant significantly. The kinetics of plasma-chemical reactions of excited molecules is determined not only by the rate constants but mostly by their mole fractions at fixed quantum-mechanical state. Figure 9(b) compares the reaction rates for typical chain branching reactions stimulated by excited molecules. As shown in figure 9(b), the vibrational and electronic excitation of molecules to higher energy levels, such as $CH_4(v)$, $O_2(v)$, and $O_2(a^1\Delta_g)$, can accelerate the reactions if the thermal equilibrium reaction path has a significant energy barrier [42, 43].

For efficient formation of a large number of excited molecules in the intermediate *E*/*N* gas discharge, significant generation of these species in the gas discharge plasma and quick quenching in collisions with major mixture components are necessary. As shown in figure 10, the concentrations of the excited species and final products in a stoichiometric mixture

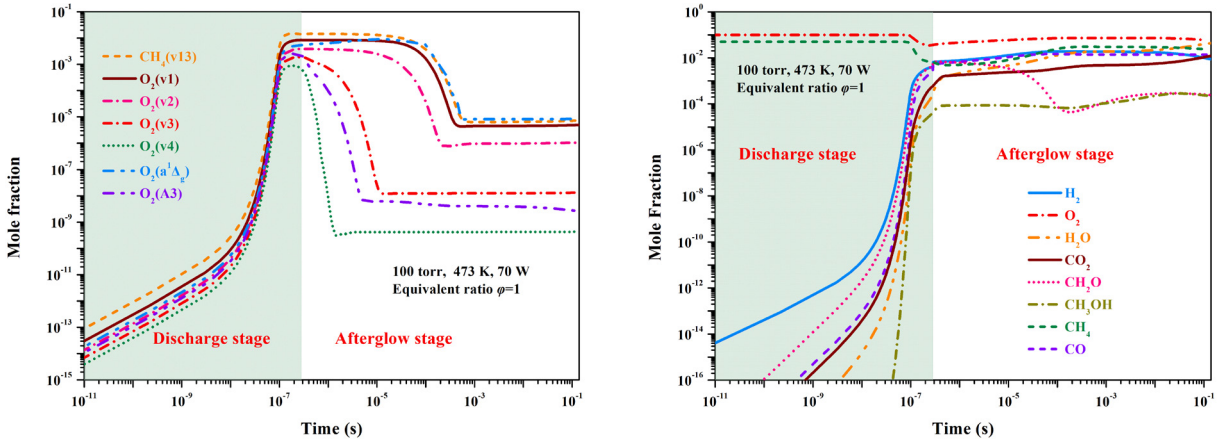

Figure 10. Time-dependent evolution of (a) excited species and (b) products in a stoichiometric mixture (0.05 CH_4/0.1 O_2/0.85 He) with an *E/N* value of 68.2 Td.

(0.05 CH_4/0.1 O_2/0.85 He) rapidly increase with discharge propagation. The concentrations of the final products are on the same order of magnitude as that of the excited species when the discharge is terminated. The excited species quickly decrease after discharge owing to the fast vibrational–translational (VT) and electronic–electronic relaxation, however, the final products continue to be produced by the ordinary chain reactions or the chain reactions stimulated by the excited species during the afterglow stage. The relaxation time of vibrational or electronic states is μs ms in an He/CH_4/O_2 discharge mixture. Comparatively, the low vibrational levels including CH_4(v13), CH_4(v24), O_2(v1), and O_2(v2) present a relatively longer relaxation time owing to their low relaxation rate constant. Despite this, the excited energy at low vibrational levels is not sufficiently high to promote significant dissociation.

3.3. Kinetics of excited species

Both the reaction path flux analysis and the sensitivity analysis of the excited species have been done for a stoichiometric mixture (0.05 CH_4/0.1 O_2/0.85 He) under the total pressure of 100 Torr and temperature of 473 K, with *E/N* value of 68.2 Td. The path fluxes obtained due to averaging by residence times for the mole fractions of the excited molecules, key radicals and final products are shown in figure 11. Note that the detailed reaction channels of the electronically excited He(2^3S), such as $He(2^3S) + CH_4 \rightarrow He + CH_4^+ + e$, $He(2^3S) + CH_4 \rightarrow H e + CH_3^+ + H + e$, $He(2^3S) + CH_4 \rightarrow He + CH_2^+ + H_2 + e$, $He(2^3S) + CH_4 \rightarrow He + CH + H_2 + H$, $He(2^3S) + O_2 \rightarrow He + O_2^+ + e$, have been included in the improved reaction set. As shown in the calculated reaction path flux in figure 11, the electronically excited He(2^3S) plays minor roles; however, the electronically and vibrationally excited species $O_2(a^1\Delta_g)$, $O(^1D)$, $O(^1S)$, CH_4(v), and O_2(v) play significant roles in ion, radical, and final product generation. As can be clearly seen in figure 11(a), the relatively lower vibrational levels of CH_4(v) and O_2(v)are due to the direct electron impact excitation $e + CH_4 \rightarrow e + CH_4(v)$, $e + O_2 \rightarrow e + O_2(v)$ and relaxation of their higher vibrational levels, i.e. $O_2(v = n) + M \rightarrow O_2(v = n - 1) + M$ (n is the vibrational level). However, for the electronically excited oxygen, $O_2(a^1\Delta_g)$, the major formation pathway is through the relaxation of its higher electronic level, i.e. $O_2(b^1\Sigma_g^+) + M \rightarrow O_2(a^1\Delta_g) + M$. From the consumption pathways in figure 11(a), the excited molecules, including CH_4(v), O_2(v), and $O_2(a^1\Delta_g)$ significantly affect the production of radicals. The consumption pathway shows that 81.7% of CH_4(v13), 58.1% of O_2(v3), and 36.6% of O_2(v4) are consumed by the relaxation reactions. Accordingly, the remaining percentages of the vibrational species participate in the chain branching reactions, leading to the formation of CH_3, OH, and O radicals. The sensitive pathway for radical generation involved by CH_4(v), O_2(v) are mainly through $CH_4(v) + O \rightarrow CH_3 + OH$, $O_2(v) + H \rightarrow O + OH$. In contrast to the vibrational species, the electronically excited oxygen, $O_2(a^1\Delta_g)$, is dominantly consumed via the reactions $O_2(a^1\Delta_g) + H \rightarrow O + OH$ and $O_2(a^1\Delta_g) + HCO \rightarrow CO + H O_2$, owing to its higher excitation energy.

For the higher vibrational or electronic levels, the energy of excitation is sufficient to reduce the activation energy barrier and further affect radical formation, such as the H and OH formation shown in figure 11(b). To be more specific, consumption of CH_4(v13), $O(^1D)$, and O_2(v) leads to 3.6%, 12.7%, and 3.8% of the OH radical formation, respectively, resulting in the formation of CO, H_2, CO_2, H_2O, CH_2O, and CH_3OH. The predicted pathway in figure 11(c) also shows that the excited species including $O(^1D)$, $O(^1S)$, CH_4(v13), and $O_2(a^1\Delta_g)$ have significant effects on product species formation, which will be qualitatively discussed later in the sensitivity analysis section. A small set of reaction schemes involving CH_4(v13), $CH_4(v13) + OH \rightarrow H_2O + CH_3$, accounts for 1.6% of the H_2O formation, indicating the kinetic role of vibrational states in a complex plasma chemistry system.

A sensitivity analysis has been performed for a stoichiometric mixture (0.05 CH_4/0.1 O_2/0.85 He) under the total pressure of 100 Torr at 473 K. Figure 12 shows the time evolution of sensitivity coefficients for the production of key excited species, i.e. CH_4(v13), O_2(v3), O (^{1}D), and $O_2(a^1\Delta_g)$. Sensitivity analysis for minor and major products as well as

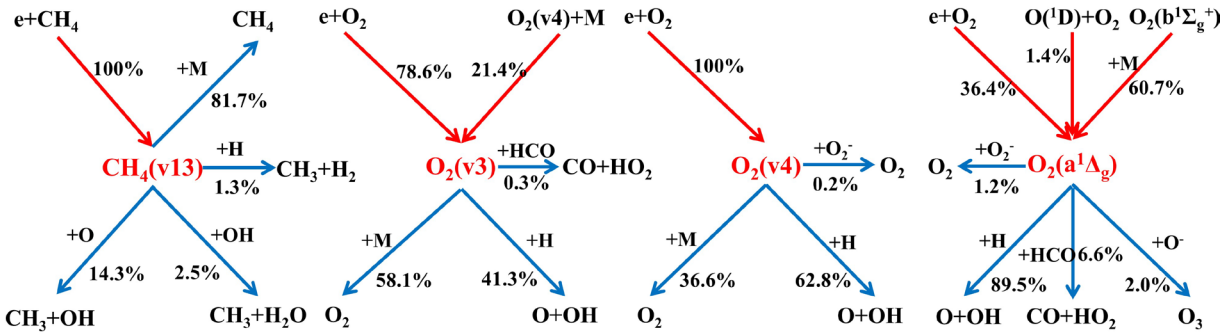

(a)

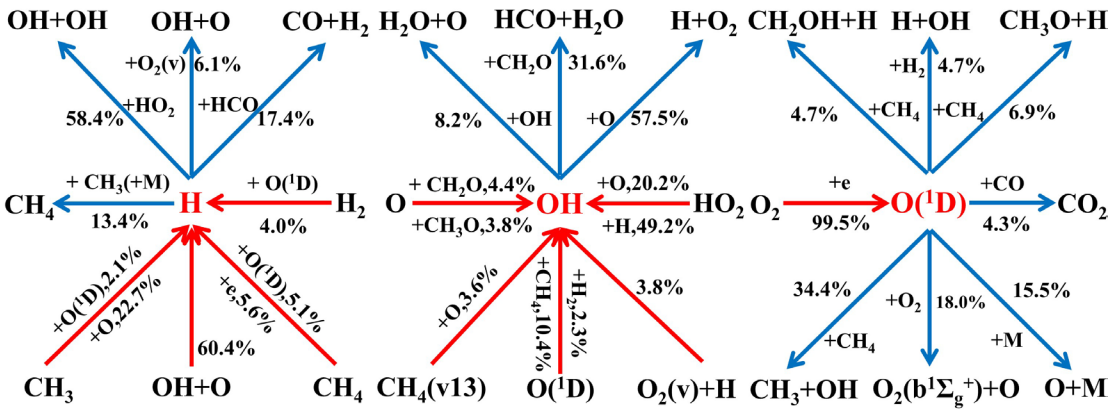

(b)

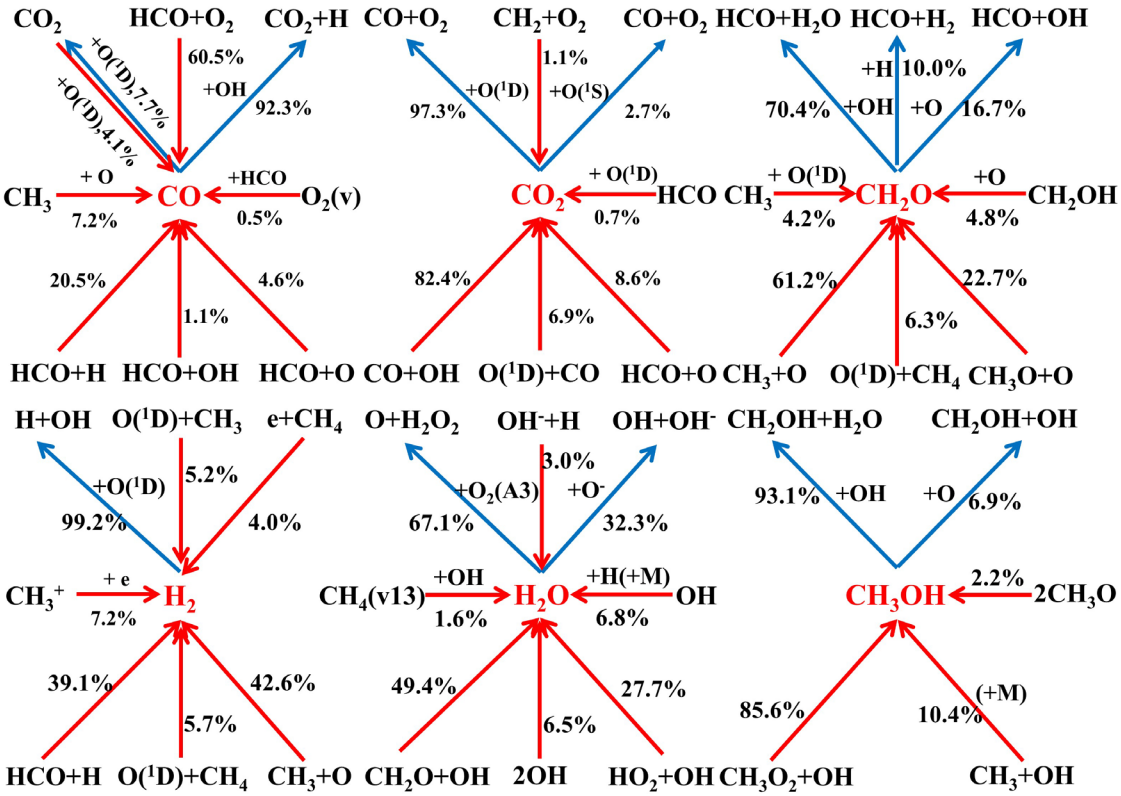

(c)

Figure 11. Path fluxes of (a) excited molecules, (b) key radicals, (c) final products. Red arrows represent the production pathways and the blue ones represent the consumption pathways. *M* is the neutral species.

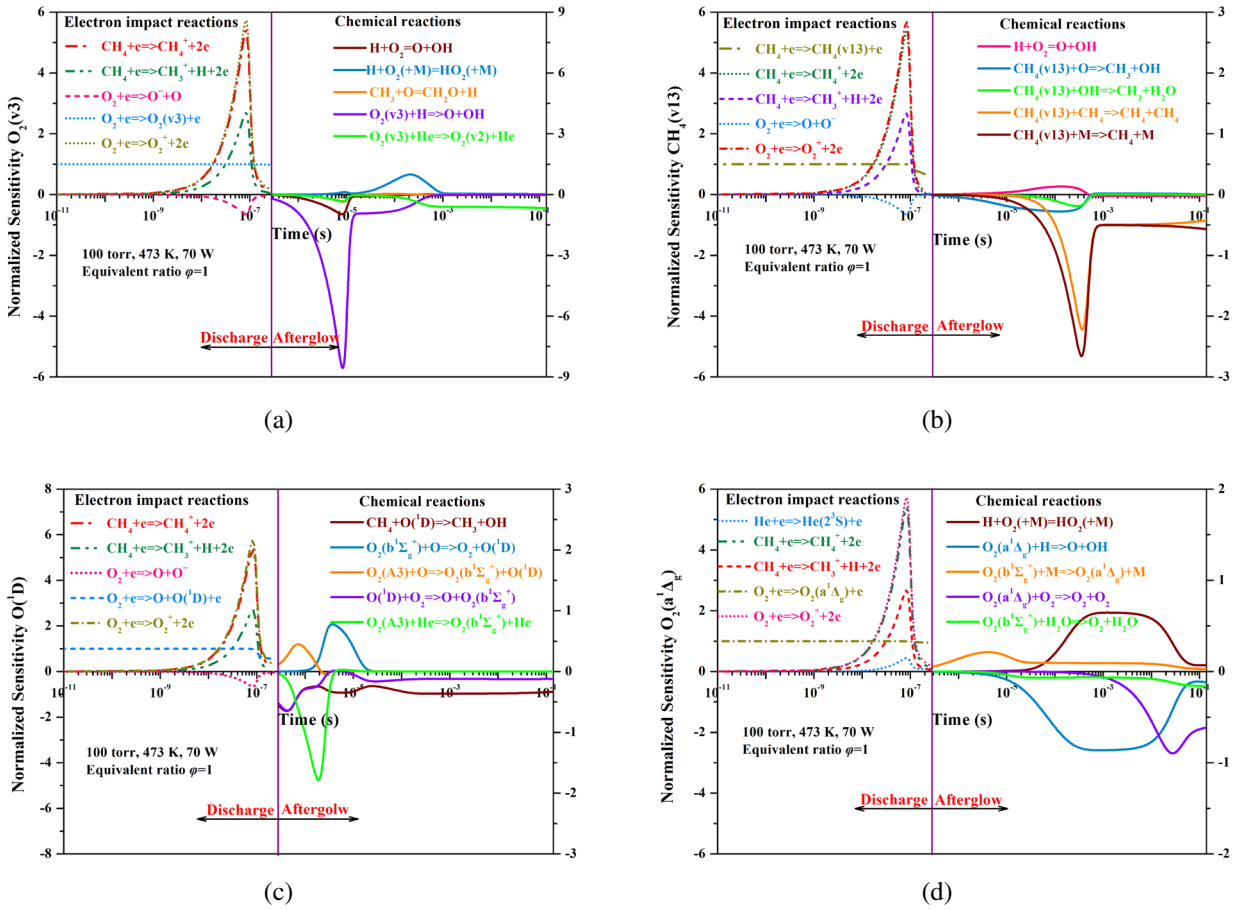

Figure 12. Differential sensitivity analysis of the excited species: (a) O_2(v3), (b) CH_4(v13), (c) $O(^1D)$, and (d) $O_2(a^1\Delta_g)$. The sensitivities of the electron impact reactions and the chemical reactions are separated left and right owing to the different scales of sensitivity coefficients at the two different stages.

active radicals has also been performed (not included in this paper). Positive sensitivity coefficient presents the promotive effects of the corresponding reactions on species production and vice versa. Obviously, the direct electron impact reactions have higher sensitivity (about 2–3 times greater than that of the chemical reactions in the sensitivity coefficients) in the formation and consumption of the excited species. This demonstrates that molecular excitation is decoupled from the low-temperature chemistry in the plasma excited reactions.

The sensitivity analysis for O_2(v3) and CH_4(v13) species again reveal the dominant roles of the direct electron impact excitation and its relaxation in the generation and consumption of the vibrationally excited species, as shown in figures 12(a) and (b). It also demonstrates that the electron impact can stimulate dissociation of molecules by vibrational excitation. Under the conditions of incomplete relaxation, vibrational species CH_4(v) and O_2(v) accelerate chain propagating reactions, such as $CH_4(v) + O \rightarrow CH_3 + OH$, $CH_4(v) + OH \rightarrow CH_3 + H_2O$, and $O_2(v) + H \rightarrow O + OH$, thus stimulating the production of active radicals and final products.

For the sensitivity plots in figure 12(c), the ionization reactions $CH_4 + e \rightarrow CH_4^+ + 2e$, $O_2 + e \rightarrow O_2^+ + 2e$, and $CH_4 + e \rightarrow CH_3^+ + H + 2e$, as well as the dissociation reactions in an RF plasma discharge, i.e. $O_2 + e \rightarrow O + O(^1D) + e$, play sensitive roles in $O(^1D)$ production. On the other hand, the excitation reactions $O_2(b^1\Sigma_g^+) + O \rightarrow O_2 + O(^1D)$ and $O_2(A3) + O \rightarrow O_2(b^1\Sigma_g^+) + O(^1D)$ help to promote $O(^1D)$ production in the discharge afterglow. Two sets of reaction schemes leading to $O(^1D)$ consumption are identified: kinetic relaxation and the chain reactions involving $O(^1D)$, $CH_4 + O(^1D) \rightarrow CH_3 + OH$, and $O(^1D) + O_2 \rightarrow O + O_2(b^1\Sigma_g^+)$, which result in the formation of a large amount of CH_3 and OH species. Thus, in an RF discharge with intermediate reduced electric fields, low-energy excitation of molecules, such as vibrational excitation and excitation of lower electronic states, are essential in the stimulation of methane oxidation and major and minor product specie production.

$O_2(a^1\Delta_g)$ is another important excited species in the oxidation of methane fuel. Similar to those of $O(^1D)$, the impact excitation, ionization, and dissociation by electrons, as well as relaxation of $O_2(b^1\Sigma_g^+)$, make great contributions to $O_2(a^1\Delta_g)$ production, as shown in figure 12(d). Additionally, the chain reaction $H + O_2(+M) = HO_2(+M)$ is also found to affect $O_2(a^1\Delta_g)$ formation. This is mainly because the consumption of H and O_2 can promote $O_2(a^1\Delta_g)$ formation. There are three different major consumption pathways for $O_2(a^1\Delta_g)$ species: the kinetic relaxation of $O_2(a^1\Delta_g)$, e.g. $O_2(a^1\Delta_g) + O_2 \rightarrow O_2 + O_2$; the chain propagating reaction involving $O_2(a^1\Delta_g)$, $O_2(a^1\Delta_g) + H \rightarrow O + OH$, which is the

most important consumption pathway; and $O_2(a^1\Delta_g)$ consumption by chain initiation reactions, e.g. $CH_4 + O_2(a^1\Delta_g) \rightarrow CH_3 + HO_2$. According to the sensitivity analysis, this pathway does not affect methane oxidation significantly.

4. Conclusion

The kinetics of pyrolysis and oxidation of CH_4 in an He/CH_4/O_2 mixture was investigated experimentally by using a low temperature DBD flow reactor. The detailed chemical kinetic reaction mechanism including a set of electron impact reactions, dissociative recombination reactions, reactions involving vibrationally- and electronically-excited species, and some important three-body recombination reactions were analyzed by mathematical modelling using a hybrid BOLSIG-CHEMKIN method. The pyrolysis and oxidation experiments revealed that the CH_4 and O_2 conversions linearly increased with the plasma power, highlighting the strong correlation between the molecular excitations and energy input. However, a non-linear trend in the CO formation was revealed with an increase in CO production at lower input energy but a decrease in the CO production at higher energy inputs. A large increase in the production of CO_2 at higher energy inputs further indicates the high plasma power promotion of the CO conversion into CO_2. It was also found that a higher plasma energy input largely inhibited CH_2O formation, but it promoted H_2O formation.

The kinetics and reaction pathways for low temperature plasma activated methane oxidation and dissociation were modelled and compared to the experimental results. Calculation of the electron energy that branched into different molecular degrees of freedom showed that the vibrational and electronic excitation processes effectively competed with the dissociation and ionization processes of gas molecules in the RF discharge with an *E*/*N* of 30–70 Td. Among the main reactions caused by electron impact, the reaction rates are as follow: dissociative excitation of oxygen, $e + O_2 \rightarrow e + O + O(^1D)$ > vibrational excitation of CH_4 > electronic excitation of O_2 > vibrational excitation ofO_2. The modelling results also revealed that relaxation of $O(^1D)$ was the fastest process among all the reactions investigated. In contrast, higher vibrational levels such as CH_4(v13), O_2(v3), and O_2(v4), present a relatively longer relaxation time owing to the large populations that are produced in an RF plasma, which facilitate the formation of active radicals. The reaction path flux as well as sensitivity analysis further revealed the dominant roles of the direct electron impact excitation and its relaxation in the generation and consumption of the vibrationally excited species.

Further comparison of the measured and numerical predicted results in an He/CH_4/O_2 combustible mixture revealed that the kinetic model captured the major trends of reactant (CH_4 and O_2) consumption and primary species products; however, it failed to accurately predict the production of hydrogen and methanol. The large discrepancy in the methanol prediction suggested that there existed a large uncertainty in the low temperature oxidation reactions. Quantitative diagnostics of intermediate species, including OH, CH_3 and CH_3O_2, are needed to provide validation targets for kinetic modelling in the future.

Supplementary material

Supplementary material associated with this article can be found, in the online version, at (stacks.iop.org/JPhysD/53/064001/mmedia).

Acknowledgments

This work was supported by the Fundamental Research Funds for the Central Universities (2018YJS141), the National Natural Science Foundation of China (No. 21676024), the Beijing Natural Science Foundation (No. 3182029), and the Advance Space Propulsion Laboratory of BICE and Beijing Engineering Research Center of Efficient and Green Aerospace Propulsion Technology (LabASP-2018-10).

ORCID iDs

Jintao Sun https://orcid.org/0000-0003-2053-1506
Qi Chen https://orcid.org/0000-0002-1783-5931

References

[1] Ju Y and Sun W 2015 Plasma assisted combustion: dynamics and chemistry *Prog. Energ. Combust.* **48** 21–83
[2] Starikovskiy A and Aleksandrov N 2013 Plasma-assisted ignition and combustion *Prog. Energ. Combust.* **39** 61–110
[3] Aleksandrov N L, Kindysheva S V and Kochetov I V 2014 Kinetics of low-temperature plasmas for plasma-assisted combustion and aerodynamics *Plasma Sources Sci. Technol.* **23** 015017
[4] Gan Y, Tong Y, Ju Y, Zhang X, Li H and Chen X 2017 Experimental study on electro-spraying and combustion characteristics in meso-scale combustors *Energy Convers. Manage.* **131** 10–7
[5] Tang J, Zhao W and Duan Y 2011 Some observations on plasma-assisted combustion enhancement using dielectric barrier discharges *Plasma Sources Sci. Technol.* **20** 045009
[6] Pipa A V, Andrasch M, Rackow K, Ehlbeck J and Weltmann K D 2012 Observation of microwave volume plasma ignition in ambient air *Plasma Sources Sci. Technol.* **21** 035009
[7] Chintala N, Meyer R, Hicks A, Bao A, Rich J W, Lempert W R and Adamovich I V 2005 Nonthermal ignition of premixed hydrocarbon-air flows by nonequilibrium radio frequency plasma *J. Propul. Power* **21** 583–90
[8] Chintala N, Bao A, Lou G and Adamovich I V 2006 Measurements of combustion efficiency in nonequilibrium RF plasma-ignited flows *Combust. Flame* **144** 744–56
[9] Kosarev I N, Khorunzhenko V I, Mintoussov E I, Sagulenko P N, Popov N A and Starikovskaia S M 2012 A nanosecond surface dielectric barrier discharge at elevated pressures: time-resolved electric field and efficiency of initiation of combustion *Plasma Sources Sci. Technol.* **21** 045012

[10] Sun W, Uddi M, Won S H, Ombrello T, Carter C and Ju Y 2012 Kinetic effects of non-equilibrium plasma-assisted methane oxidation on diffusion flame extinction limits *Combust. Flame* **159** 221–9
[11] Lefkowitz J K, Uddi M, Windom B C, Lou G and Ju Y 2014 *In situ* species diagnostics and kinetic study of plasma activated ethylene dissociation and oxidation in a low temperature flow reactor *Proc. Combust. Inst.* **35** 3505–12
[12] Fridman A 2008 *Plasma Chemistry* (New York: Cambridge University Press)
[13] Ombrello T, Won S H, Ju Y and Williams S 2010 Flame propagation enhancement by plasma excitation of oxygen. Part II: effects of $O_2(a^1\Delta_g)$ *Combust. Flame* **157** 1916–28
[14] Popov N A 2016 Kinetics of plasma-assisted combustion: effect of non-equilibrium excitation on the ignition and oxidation of combustible mixtures *Plasma Sources Sci. Technol.* **25** 043002
[15] Uddi M, Jiang N, Mintusov E, Adamovich I V and Lempert W R 2009 Atomic oxygen measurements in air and air/fuel nanosecond pulse discharges by two photon laser induced fluorescence *Proc. Combust. Inst.* **32** 929–36
[16] Starikovskaia S M, Anikin N B, Kosarev I N, Popov N A and Starikovskii A Y 2006 Analysis of ignition by nonequilibrium sources. Ignition of homological series of hydrocarbons by volume nanosecond discharge *44th AIAA Aerospace Sciences Meeting and Exhibition, AIAA 2006-616 (Reno, NE, 9–12 January 2006)* (https://doi.org/10.2514/6.2006-616)
[17] Popov N A 2007 The effect of nonequilibrium excitation on the ignition of hydrogen–oxygen mixtures *High Temp.* **45** 261–79
[18] Stancu G D, Kaddouri F, Lacoste D A and Laux C O 2010 Atmospheric pressure plasma diagnostics by OES, CRDS and TALIF *J. Phys. D: Appl. Phys.* **43** 124002
[19] Adamovich I V, Li T and Lempert W R 2015 Kinetic mechanism of molecular energy transfer and chemical reactions in low-temperature air-fuel plasmas *Phil. Trans.* A **373** 61–6
[20] Montello A, Yin Z, Burnette D, Adamovich I V and Lempert W R 2013 Picosecond CARS measurements of nitrogen vibrational loading and rotational/translational temperature in nonequilibrium discharges *J. Phys. D: Appl. Phys.* **46** 464002
[21] Starik A M, Loukhovitski B I, Sharipov A S and Titova N S 2010 Intensification of shock-induced combustion by electric-discharge-excited oxygen molecules: numerical study *Combust. Theory Model.* **14** 653–79
[22] Starik A and Sharipov A 2011 Theoretical analysis of reaction kinetics with singlet oxygen molecules *Phys. Chem. Chem. Phys.* **13** 16424–36
[23] Sharipov A S and Starik A M 2012 Theoretical study of the reaction of ethane with oxygen molecules in the ground triplet and singlet delta states *J. Phys. Chem.* A **116** 8444–54
[24] Starik A M, Sharipov A S and Titova N S 2010 Intensification of syngas ignition through the excitation of CO molecule vibrations: a numerical study *J. Phys. D: Appl. Phys.* **43** 245501
[25] Tsolas N, Yetter R A and Adamovich I V 2017 Kinetics of plasma assisted pyrolysis and oxidation of ethylene. Part 2: kinetic modeling studies *Combust. Flame* **176** 462–78
[26] DeFilippo A C and Chen J Y 2016 Modeling plasma-assisted methane–air ignition using pre-calculated electron impact reaction rates *Combust. Flame* **172** 38–48
[27] Mao X, Rousso A, Chen Q and Ju Y 2019 Numerical modeling of ignition enhancement of CH_4/O_2/He mixtures using a hybrid repetitive nanosecond and DC discharge *Proc. Combust. Inst.* **37** 5545–52
[28] Mao X and Chen Q 2018 Effects of vibrational excitation on nanosecond discharge enhanced methane–air ignition *AIAA J.* **56** 4312–20
[29] Togai K, Tsolas N and Yetter R A 2016 Kinetic modeling and sensitivity analysis of plasma-assisted oxidation in a H_2/O_2/Ar mixture *Combust. Flame* **164** 239–49
[30] Anikin N B, Starikovskaia S M and Starikovski A Y 2006 Oxidation of saturated hydrocarbons under the effect of nanosecond pulsed space discharge *J. Phys. D: Appl. Phys.* **39** 3244–52
[31] Chen Q, Yang X, Sun J, Zhang X, Mao X, Ju Y and Koel B E 2017 Pyrolysis and oxidation of methane in a RF plasma reactor *Plasma Chem. Plasma Process.* **37** 1551–71
[32] Sun J and Chen Q 2019 Kinetic roles of vibrational excitation in RF plasma assisted methane pyrolysis *J. Energy Chem.* **39** 188–97
[33] LXcat 2010 www.lxcat.laplace.univ-tlse.fr
[34] Straub H C, Lin D, Lindsay B G, Smith K A and Stebbings R F 1997 Absolute partial cross sections for electron-impact ionization of CH_4 from threshold to 1000 eV *J. Chem. Phys.* **106** 4430–5
[35] Janev R K and Reiter D 2002 Collision processes of CH_y and CH_y^+ hydrocarbons with plasma electrons and protons *Phys. Plasmas* **9** 4071–81
[36] Shen X, Yang X, Santner J, Sun J and Ju Y 2015 Experimental and kinetic studies of acetylene flames at elevated pressures *Proc. Combust. Inst.* **35** 721–8
[37] Zhao H, Fu J, Francis M H and Ju Y 2017 Effect of prompt dissociation of formyl radical on 1,3,5-trioxane and CH_2O laminar flame speeds with CO_2 dilution at elevated pressure *Combust. Flame* **183** 253–60
[38] Starikovskiy A and Aleksandrov N 2017 Mechanism of plasma-assisted ignition for H_2 and C1–C5 hydrocarbons *55th AIAA Aerospace Sciences Meeting, AIAA 2017-1997 (Grapevine, TE, 9–13 January 2017)* (https://doi.org/10.2514/6.2017-1977)
[39] Capitelli M 2000 *Plasma Kinetics in Atmospheric Gases* (Berlin: Springer)
[40] Levine R D and Bernstein R B 1976 *Dynamics of Molecular Collisions* (Boston, MA: Springer)
[41] Law C K 2006 *Combustion Physics* (New York: Cambridge University Press)
[42] Kozák T and Bogaerts A 2014 Splitting of CO_2 by vibrational excitation in non-equilibrium plasmas: a reaction kinetics model *Plasma Sources Sci. Technol.* **23** 045004
[43] Kozák T and Bogaerts A 2015 Evaluation of the energy efficiency of CO_2 conversion in microwave discharges using a reaction kinetics model *Plasma Sources Sci. Technol.* **24** 015024